Metal Nanoparticle/Ionic Liquid/Cellulose: New Catalytically Active Membrane Materials for Hydrogenation Reactions

Marcos A. Gelesky,[†,‡] Carla W. Scheeren,[†] Lucas Foppa,[†] Flavio A. Pavan,[†,§] Silvio L. P. Dias,[†] and Jairton Dupont*[,†]

Institute of Chemistry, UFRGS, Porto Alegre - RS - Brazil, UNIPAMPA, Universidade Federal do Pampa, Bagé - RS - Brazil, and Institute of Chemistry and Biotechnology, UFAL, Universidade Federal de Alagoas, Maceió - AL - Brazil

Received March 16, 2009; Revised Manuscript Received April 22, 2009

Transition metal-containing membrane films of 10, 20, and 40 μm thickness were obtained by the combination of irregularly shaped nanoparticles with monomodal size distributions of 4.8 ± 1.1 nm (Rh(0)) and 3.0 ± 0.4 nm (Pt(0)) dispersed in the ionic liquid (IL) 1-*n*-butyl-3-methylimidazolium bis(trifluoromethane sulfonyl)imide (BMI·$(NTf)_2$) with a syrup of cellulose acetate (CA) in acetone. The Rh(0) and Pt(0) metal concentration increased proportionally with increases in film thickness up to 20 μm, and then the material became metal saturated. The presence of small and stable Rh(0) or Pt(0) nanoparticles induced an augmentation in the CA/IL film surface areas. The augmentation of the IL content resulted in an increase of elasticity and decrease in tenacity and toughness, whereas the stress at break was not influenced. The introduction of IL probably causes an increase in the separation between the cellulose macromolecules that results in a higher flexibility, lower viscosity, and better formability of the cellulose material. The nanoparticle/IL/CA combinations exhibit an excellent synergistic effect that enhances the activity and durability of the catalyst for the hydrogenation of cyclohexene. The nanoparticle/IL/cellulose acetate film membranes display higher catalytic activity (up to 7353 h^{-1} for the 20 μm film of CA/IL/Pt(0)) and stability than the nanoparticles dispersed only in the IL.

Introduction

Supported ionic liquid phase (SILP) is emerging as an interesting protocol for the immobilization of transition metal catalysts since it may combine the advantages of ionic liquids (IL) with those of heterogeneous support materials.[1,2] In particular, the combination of an IL with a solid support material may have several advantages, such as potentially using fixed-bed reactors for continuous reactions,[3−7] reducing IL levels, and allowing for a facile and efficient separation of products from catalyst. Moreover, in comparison to traditional liquid−liquid biphasic systems, higher catalytic activity and lower metal leaching can be achieved by appropriately tuning the experimental conditions.[2,8−12]

These materials are prepared by the covalent attachment of IL to the support surface or by simply depositing the IL phases containing catalytically active species, usually transition metal complexes[4] or, more rarely, metal nanoparticles[13] on the surface of the support, which is usually a silica-based or polymeric material. However, as in classical heterogeneous catalysis, the use of active polymeric membranes[14−18] has received little attention when compared with catalytically active inorganic membranes.[19−22] This can be attributed to the need to perform reactions in multiphase conditions at elevated temperatures that undermine the stability of the organic membrane. However, inorganic membranes (albeit with high chemical and thermal stability)[23] may be substituted by less expensive and more versatile polymeric organic membranes. The main characteristic of a membrane is its porous structure, which selectively allows components to pass from one side to the other.[15] Moreover, the unique structure of the catalytic polymeric membranes may have other additional advantages such as immobilizing more active and selective nanoscale catalysts with a reduction in particles loss, prevention of nanoparticles agglomeration, and the establishment of a porous contact region between gas and liquid phases within the membrane structure.[24] Therefore, the combination of metal nanoparticles dispersed in an IL with a polymeric organic membrane such as cellulose derivatives[25−30] may generate new and versatile catalytic materials.[31] Indeed, we report that the association of rhodium[32] and platinum[33] nanoparticles with 1-*n*-butyl-3-methylimidazolium bis(trifluoromethane sulfonyl)imide (BMI.$(NTf)_2$) and cellulose acetate generates new membrane-supported metal hydrogenation catalysts.

Experimental Section

General. All reactions involving platinum and rhodium nanoparticles were carried out under an argon atmosphere in modified Fischer−Porter Bottles. The halide-free 1-*n*-butyl-3-methylimidazolium tetrafluoroborate (BMI·BF_4) and BMI·$N(Tf)_2$ IL were prepared according to a known procedure and dried over molecular sieves (4 Å). Their purity was checked by ^{1}H NMR using the intensity of the ^{13}C satellites of the imidazolium N-methyl group as an internal standard.[34] Solvents were dried with the appropriate drying agents and distilled under argon prior to use. Cellulose acetate (Aldrich, 39.8% wt of acetylation content) and acetone (Merck, 99.8%) were used to prepare the membrane-supported nanoparticles. All other chemicals were purchased from commercial sources and used without further purification. NMR spectra were recorded on a Varian Inova 300 spectrometer. Infrared spectra were performed on a Bomem B-102 spectrometer. Mass spectra were obtained using a GC/MS Shimadzu QP-5050 (EI, 70 eV). Gas chromatography analysis was performed with a Hewlett-Packard-5890 gas chromatograph with an FID and a 30 m capillary column with a dimethylpolysiloxane stationary phase. The nanoparticle formations

* To whom correspondence should be addressed. Fax: (+55) 51 33087304. E-mail: jairton.dupont@ufrgs.br.
† UFRGS.
‡ UFAL.
§ UNIPAMPA.

10.1021/bm9003089 CCC: $40.75
Published on Web 05/12/2009

were carried out in a modified Fischer−Porter bottle immersed in a silicone oil bath while connected to a hydrogen tank. The temperature was maintained at 75 °C with a hot-stirring plate connected to a digital controller (ETS-D4 IKA).

Synthesis and Isolation of Rh(0) Nanoparticles. Rh(0) nanoparticles were prepared by simple hydrogen reduction (4 atm H_2, constant pressure) of 0.026 g (0.1 mmol) of $RhCl_3 \cdot nH_2O$ dissolved in 1-*n*-butyl-3-methylimidazolium tetrafluoroborate ($BMI \cdot BF_4$) at 75 °C for 1 h to yield a black suspension. Acetone (15 mL) was then added, and centrifugation of this mixture yielded nanoparticles of 4.8 ± 1.1 nm, which were washed with acetone and dried under reduced pressure (see Figures S1 and S2).

Synthesis and Isolation of Pt(0) Nanoparticles. Pt(0) nanoparticles were prepared by simple hydrogen decomposition (4 atm H_2, constant pressure) of 0.054 g (0.1 mmol) of $Pt_2(dba)_3$ dissolved in $BMI \cdot BF_4$ at 75 °C for 1.5 h to yield a black suspension. Acetone (15 mL) was added, and centrifugation of this mixture yielded nanoparticles of 3.0 ± 0.4 nm, which were washed with acetone and dried under reduced pressure.

Preparation of a Polymeric Catalytic Membrane Reactor Containing Rh(0) and Pt(0) Nanoparticle-Doped $BMI \cdot N(Tf)_2$. Cellulose acetate (10.0 g) was added to a reaction flask containing 90 mL of acetone, and the mixture was allowed to sit for 24 h at room temperature under a dry nitrogen atmosphere. After a viscous syrup was formed, 10.0 mg (0.1 mmol) of Rh(0) or 10.0 mg (0.05 mmol) of Pt(0) nanoparticles dispersed in 1.0 g of $BMI \cdot N(Tf)_2$ were added to 5.0 g of the syrup, respectively. The mixtures were magnetically stirred until a homogeneous phase was obtained. Films of the membrane reactors, designated here as CA/IL/Rh(0) and CA/IL/Pt(0), respectively, were prepared by spreading the homogeneous phase over a glass plate. The thickness was controlled to 10, 20, and 40 μm by using a spacer. The solvent was evaporated in an open atmosphere for 2 min. A similar method was used to prepare blank CA films, except that no Rh(0) or Pt(0) nanoparticles were used.[35−38] The films containing Rh(0) or Pt(0) nanoparticles were used in the hydrogenation reactions of cyclohexene.

X-ray Powder Diffraction Analysis (XRD). The phase structures of the Pt(0) and Rh(0) nanoparticles prepared in $BMI \cdot BF_4$ were characterized by XRD. For the XRD analysis, the platinum nanoparticles were isolated as a fine powder and placed in the sample holder. The XRD experiments were carried out on a Siemens D500 diffractometer equipped with a curved graphite crystal using Cu Ka radiation (λ=1.5406 Å). The diffraction data were collected at room temperature in a Bragg−Brentano $\theta-2\theta$ geometry. The equipment was operated at 40 kV and 20 mA with a scan range between 20 and 90°. The diffractograms were obtained with a constant step of $\Delta 2\theta = 0.05$. The indexation of Bragg reflections was obtained with a pseudo-Voigt profile fitting using the FULLPROF code.

Scanning Electron Microscopy (SEM) and EDS Elemental Analysis. The morphology of the polymeric films CA/IL/Pt(0) or CA/IL/Rh(0) and the electron dispersive spectroscopy (EDS) analysis were performed using a JEOL model JSM 5800 with 10 and 20 kV and magnification of 3000−10000×.

Transmission Electron Microscopy Analysis (TEM). TEM was obtained using a JEOL JEM 2010 microscope operating at 200 kV equipped with an EDS system and a JEOL JEM1200EXII operating at 120 kV. A 20 μm objective aperture and slightly under focused ($\triangle f \approx$ −300 nm) objective lens were used to obtain the bright field TEM images.

The morphology and electron diffraction (ED) of the isolated platinum nanoparticles immobilized in the membrane were analyzed by TEM. The samples were prepared by deposition of the Rh(0) or Pt(0) nanoparticles in isopropanol at room temperature on a carbon-coated copper grid. The histograms of the nanoparticle size distribution were obtained from measurements of around 300 diameters and were reproduced in different regions of the Cu grid, assuming a spherical shape (see Figure S2). For the analyses the nanoparticles of Rh(0) or Pt(0) immobilized in the cellulose membrane, the material was immobilized in resin and sliced with the technique of ultramicrotomy and placed on a carbon-coated copper grid.

N_2 Adsorption−Desorption Isotherms. The specific surface area and pore size distribution of the CA/IL/Rh(0) and CA/IL/Pt(0) polymeric films were determined at nitrogen boiling point in a homemade volumetric apparatus with a vacuum line system employing a turbo molecular Edward vacuum pump, operating with temperature of 110 °C during 2 h. The pressure measurements were made using a capillary Hg barometer. The specific surface areas of the CA/IL/Rh(0) and CA/IL/Pt(0) polymeric films were determined from the BET multipoint method.[39] The pore size distribution was obtained using the BJH method.[39,40]

Infrared Analysis (IR). The infrared spectra of the pure cellulose acetate film and cellulose acetate film containing Rh(0) or Pt(0) in $BMI \cdot N(Tf)_2$ were obtained using a Shimadzu FTIR, model 8300. The spectra were obtained at room temperature with a resolution of 4 cm^{-1} and 100 cumulative scans.

Mechanical Properties. The stress−strain behaviors of the CA/IL/Rh(0) and CA/IL/Pt(0) films were analyzed by the module of a Dynamic Mechanical Analyzer (DMA Q800 V7.0), TA Instruments, using tension film geometry under isothermal temperature conditions (35 °C). These experiments were performed using a control rate force (2 $N \cdot min^{-1}$) with an upper force limit of 20.00 N in films with a rectangular shape. The Young's modulus, tensile stress, and strain to break were calculated from the stress−strain curves obtained from the measurement.

Flame Atomic Absorption (FAAS). Rhodium and platinum present in the CA/IL/Rh(0) and CA/IL/Pt(0) films were measured using a Perkin-Elmer (Boston, MA) flame atomic absorption spectrometer, model Analyst 200 (FAAS), using an air-acetylene (10:2.5 L min^{-1}) flame under optimized conditions. Hollow cathode lamps of Rh (λ = 343.5 nm) and Pt (λ = 265.9 nm) from the same manufacturer were used as radiation sources.

Hydrogenation Reactions. The hydrogenation reactions of cyclohexene with CA/IL/Rh(0) and CA/IL/Pt(0) films were carried out in a modified Fischer−Porter Bottle immersed in a silicon oil bath connected to a hydrogen tank. The fall in the hydrogen pressure in the tank was monitored with a pressure transducer interfaced through a Novus converter to a PC, and the data workup was performed with Microcal Origin 5.0 software. For the hydrogenation reaction, 210 mg of CA/IL/Rh(0) or CA/IL/Pt(0) membrane was utilized in the reactor. The membrane reactor was placed in a Fischer−Porter Bottle, and cyclohexene (1.0 g, 12.5 mmol) was added. The reactor was placed in an oil bath at 75 °C, and hydrogen was admitted into the system at constant pressure (4 atm H_2). The organic products were removed by simple decantation and analyzed by GC.

Results and Discussion

The Rh and Pt nanoparticles were prepared by the reduction of $RhCl_3$ or decomposition of $Pt_2(dba)_3$ dispersed in $BMI \cdot BF_4$ at 75 °C under 4 atm of hydrogen, as described earlier. These nanoparticles were isolated from the IL and characterized by XRD (Figure S1) and TEM analysis (Figure S2).

The nanoparticles were irregularly shaped with a monomodal size distribution of 4.8 ± 1.1 nm and 3.0 ± 0.4 nm for Rh(0)[32] and Pt(0),[33] respectively (Figure S2). They were redispersed in $BMI \cdot N(Tf)_2$ and transferred as a syrup in cellulose acetate (CA) in acetone. The homogeneous solution thus formed was spread over a glass plate, and films of 10, 20, and 40 μm thickness were obtained using a spacer. The films of the membrane reactors, CA/IL/Rh(0) and CA/IL/Pt(0), were characterized, and their mechanical and catalytic properties were investigated. For comparison, films containing the nanoparticles without the IL were also prepared.

The scanning electron micrographs (SEM) of the cross sections of the CA/IL/Rh(0) and CA/Rh(0) and CA/IL/Pt(0) and CA/Pt(0) polymeric films are shown in Figures 1 and 2,

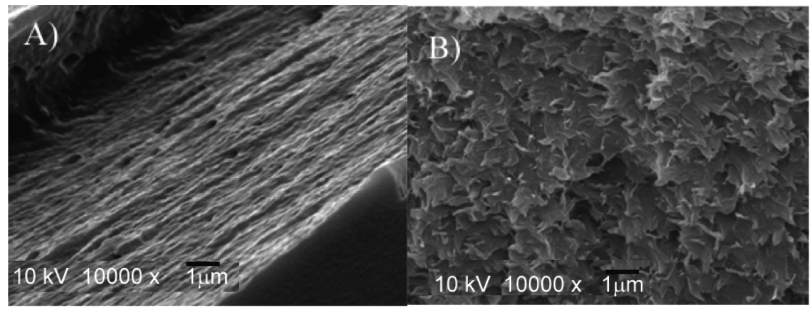

Figure 1. SEM micrographs illustrating the heterogeneous distribution on polymeric films of (A) CA/IL/Rh(0) and (B) CA/Rh(0).

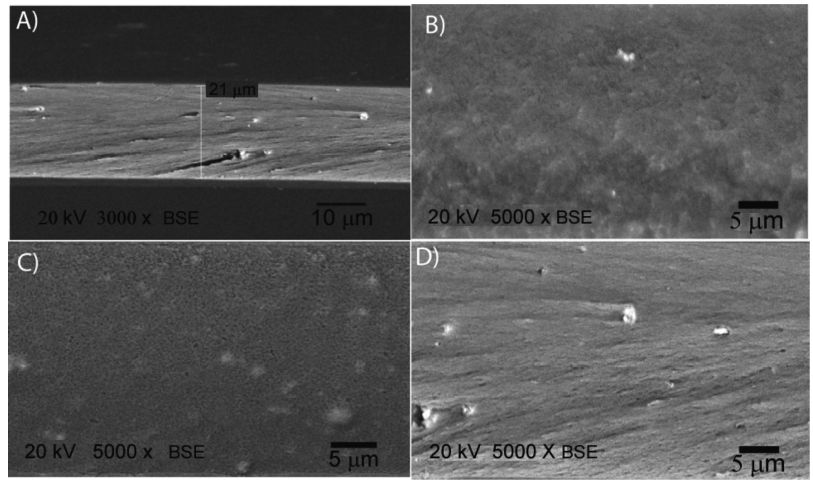

Figure 2. SEM micrographs illustrating the heterogeneous distribution on polymeric films of (A) thickness of CA/IL/Pt(0), (B) compact membrane of CA/Pt(0), (C) CA/IL/Pt(0) showing membrane porosity, and (D) CA/IL/Pt(0) showing that the membrane is also ordered in the longitudinal direction.

respectively. It is clear that the morphological structure of the films changes with or without the presence of IL. In particular, the CA/Rh(0) film (Figure 1B) seems to have a scaled and porous structure. In contrast, addition of the IL seems to cause an increase in the microstructural order in the longitudinal direction for both the CA/IL/Rh(0) (Figure 1A) and CA/IL/Pt(0) (Figure 2D) films. This result is in agreement with the general concept that imidazolium IL tend to act as entropic drivers for the formation nanostructured materials.[34,35]

Figures 1 and 2 show that the CA/IL/Rh(0) and CA/IL/Pt(0) films exhibit a skin that is relatively porous on the top side and a relatively porous structure over all of the film cross sections.

Figure 2B shows that the sample prepared in the absence of the IL also stains heterogeneously over all of the membrane cross-section, indicating the presence of Pt(0) nanoparticles (represented by the clear points (BSE method)). In the same Figure 2A, the CA/IL/Pt(0) film cross-section shows that the thickness of the film was about 21 μm. EDS analysis for Pt(0) or Rh(0) nanoparticles (Figure S3) showed the presence of the metal (Pt or Rh). EDS analysis of CA/IL/Pt(0) (Figure S4) showed S and F signals, indicating the presence of the nanoparticles and BMI.N(Tf)$_2$ in the film.

The BET surface areas of the films (20 μm) obtained in CA (5 g), CA/IL/Rh(0), and CA/IL/Pt(0) are summarized in Table 1.

The surface area of the pure cellulose acetate film containing 0.5 g of BMI·N(Tf)$_2$ was 38 m^2/g ($\pm$10%) and that of the film with 1.0 g was 24 m^2/g ($\pm$10%), demonstrating a reduction in the superficial area when the amount of IL was doubled. This result suggests that an additional increment of BMI·N(Tf)$_2$ produces an occupation of the free porous arrangement in the polymeric membrane, especially in the predominant fraction. The N_2 adsorption−desorption isotherms at very low relative pressures (Pie/Po < 0.2) exhibited high adsorption, confirming the presence of microporous structures. In the case of the cellulose acetate polymeric membrane containing Rh(0) and Pt(0) nanoparticles dispersed in the IL, surface areas of 113 m^2/g ($\pm$10%) and 96 m^2/g ($\pm$10%) were obtained, respectively. This indicates that the presence of small and stable Rh(0) or Pt(0) nanoparticles induces an augmentation in the IL/cellulose acetate film surface area (compare entries 1 and 2 with 3 and 4, Table 1).

Table 1. Surface Areas and Pore Volumes of the Films (20 μm) of Pure Cellulose Acetate Membranes and Cellulose Acetate Modified Membranes[a]

entry	sample	M(0) (mg)	IL (g)	[a]S_{bet} (m^2/g)
1	CA/IL/Rh(0)	10	1.0	113
2	CA/IL/Pt(0)	10	1.0	96
3	CA/IL	0	0.5	38
4	CA/IL	0	1.0	24

[a] With M(0) nanoparticle-doped BMI·N(Tf)$_2$.

TEM micrographs of the membranes (20 μm) containing the metal nanoparticles in the presence of the IL (Figure 3) show that the metals are distributed all over the membrane but are more homogeneously distributed in the case of Pt(0). This is a clear indication that the immobilization of the nanoparticles does not significantly change the aggregation and size distribution of the nanoparticles in the IL.

The investigation of the rhodium and platinum elemental concentrations in the catalytic polymeric membrane samples containing 1.0 g of BMI·N(Tf)$_2$ are shown in Table 2. The concentrations of Rh(0) and Pt(0) nanoparticles incorporated

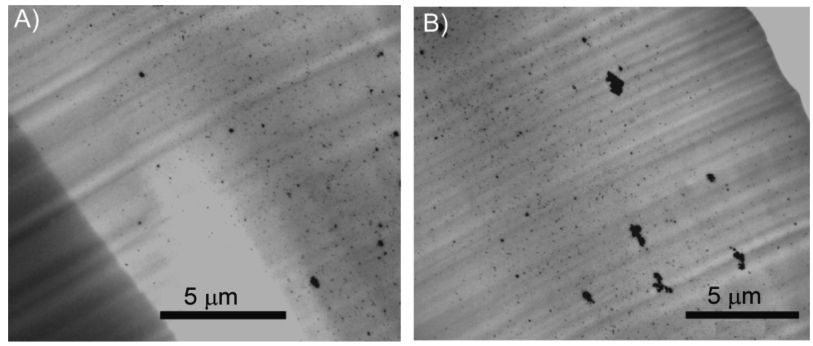

Figure 3. TEM micrographs of (A) CA/IL/Pt(0) and (B) CA/IL/Rh(0) membranes (20 μm) prepared using 0.5 g of the IL.

Table 2. Rh(0) and Pt(0) Concentrations ($\mu g \cdot g^{-1}$) and Values in % (m/m) in the Polymeric Catalytic Membrane Reactor Containing 1.0 g of BMI·N(Tf)$_2$[a]

entry	sample	thickness (μm)	M(0) ($\mu g \cdot g^{-1}$)	M(0) % (m/m)
1	CA/IL/Rh(0)	10	437	0.04
2	CA/IL/Rh(0)	20	773	0.08
3	CA/IL/Rh(0)	40	816	0.08
4	CA/IL/Pt(0)	10	432	0.04
5	CA/IL/Pt(0)	20	762	0.08
6	CA/IL/Pt(0)	40	819	0.07

[a] Determined by FAAS. Analysis conditions: air-acetylene (10:2.5 L min^{-1}); cathode lamp of Rh (λ = 343.5 nm) and Pt (λ = 265.9 nm).

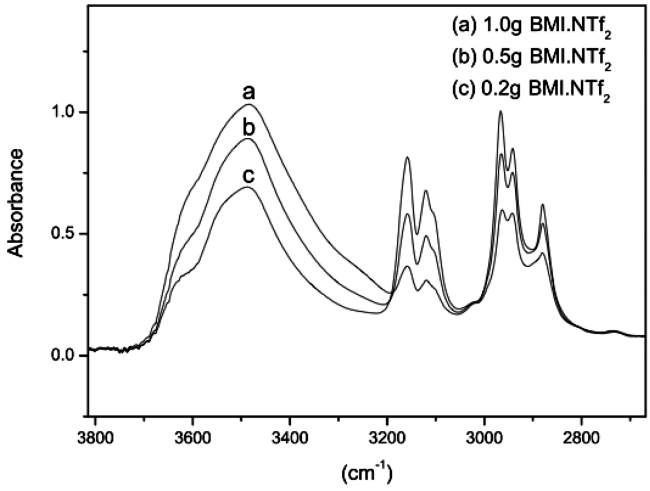

Figure 4. Infrared spectra of the cellulose acetate membranes containing Rh(0) or Pt(0) dispersed in different amounts of BMI·N(Tf)$_2$.

in the films was determined using FAAS. The concentrations are expressed as $\mu g \cdot g^{-1}$ and % (m/m) for Rh(0) and Pt(0) nanoparticles at the three thicknesses, 10, 20, and 40 μm. It is evident that the Rh(0) and Pt(0) metal concentration increased proportionally with increases in the film thickness up to 20 μm, after which, the material became saturated. The metal concentration in the membrane is therefore controlled by the amount of the ionic liquid (at >1.0 g of ionic liquid per 5.0 g of CA the ionic liquid dissolves the cellulose).

The IR spectra of the cellulose acetate membranes with the same quantity of IL did not change in the presence of Rh(0) or Pt(0). Figure 4 shows the infrared spectra of the cellulose acetate membranes containing different amounts of the IL BMI·N(Tf)$_2$.

The presence of the IL in the support was confirmed by the stretching band at 3170 cm^{-1} that is due to presence of aromatic C−H groups. After impregnation of the IL in the membrane supports, a significant decrease is observed in the intensity of the band at 3400 cm^{-1}, attributed to the −OH stretching of the pure cellulose acetate, indicating participation of the −OH group in the interaction with the IL (see Figure S5).

The tensile stress versus strain at break curves of the pure and modified cellulose acetate membranes are shown in Figure 5a and b, respectively. Some of the main parameters that can influence the stress−strain curve profiles are the polymer structure, molecular weight, degree of cross-linking, chain orientation, ionic interaction, processing conditions, and temperature, among others.

The stress tensile versus strain curves supply important information about Young's modulus (slope of linear region of the plot), tenacity, stress, and strain at the break of polymeric films. Table 3 shows the results obtained in experiments by applying a tensile force at a uniform rate to a polymeric film at a constant temperature. Figure 5a,b shows the stress−strain curve profiles for different compositions of cellulose acetate membranes submitted to a controlled force mode. In Figure 5a, the stress−strain curves are similar for the CA/Rh(0), CA-1.0 g IL, CA-1.0 g/10 mg Pt(0), and CA-1.0 g/10 mg Rh(0) membranes when compared to the pure CA membrane. These results indicate an increase of elasticity, decreases of tenacity and toughness (area under the stress−strain curve), and reduction of Young's modulus for the CA/Rh(0), CA-1.0 g IL, CA-1.0 g/10 mg Pt(0), and CA-1.0 g/10 mg Rh(0) membranes, according to Table 3. The CA/Rh(0) membrane behavior could be interpreted as a consequence of possible further agglomeration of Rh(0) nanoparticles in the CA/Rh(0) film in the absence of IL. The plasticizer effect of IL BMI·N(Tf)$_2$ in the CA-1.0 g IL membrane reduces the intermolecular forces that are usually present in the cellulose acetate. In other words, it is possible that the bis(trifluoromethane sulfonyl)imide anion of the IL strongly interacts with the hydrogen bond networks formed in the cellulose acetate chains through the nitrogen atom.[41] These results are corroborated by the infrared spectra (see below) of the cellulose acetate membrane containing Rh(0) or Pt(0) nanoparticles dispersed in IL BMI·N(Tf)$_2$. The stress−strain curve profiles of the CA-1.0 g IL-Rh(0) and CA-1.0 g IL-Pt(0) polymeric films are shown in Figure 5A. It is observed that the initial slope (Young's modulus) decreases with a decrease of the average diameter of 4.8 and 3.0 nm for Rh(0) and Pt(0) nanoparticles, respectively, and consequently, the degree of elasticity of the CA-1.0 g IL-Pt(0) film is larger compared to the CA-1.0 g IL-Rh(0) film. Figure 5B exhibits the range of IL quantified in the CA/IL/Pt(0) film membrane composition. The stress−strain curve profiles suggest that increases in IL lead to drastic decreases in Young's modulus and the elongation at break. However, the stress at break was not influenced by the IL content in the case of the Pt(0) samples (see entries 2−4). This indicates that an increase of the distance between two

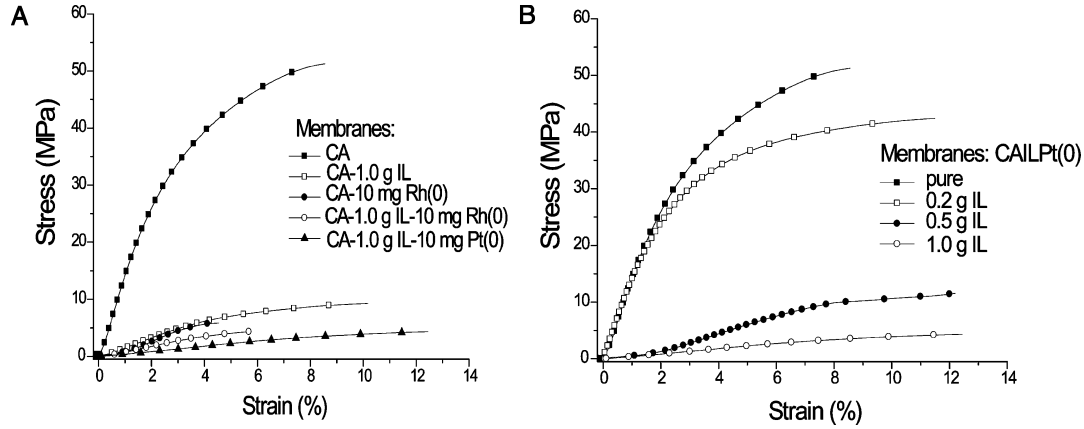

Figure 5. Stress tensile versus strain curves of the modified membranes: (a) effect of different compositions on the preparation of the cellulose acetate membranes; (b) change in the amount of IL in the composition of the cellulose acetate membrane.

Table 3. Mechanical Properties of Cellulose Acetate-Modified Membranes[a]

entry	sample	Young' modulus (MPa)	tenacity (J)	stress at break (%)	strain at break (MPa)
1	CA	1475	6.1	8.5	51
2	CA/0.2gIL/Pt(0)	1206	6.1	11.5	42.4
3	CA/0.5gIL/Pt(0)	261	1.8	12.2	11.6
4	CA/1.0gIL/Pt(0)	43	0.7	12.4	4.3
5	CA/1.0gIL	159	1.1	10.2	9.3
6	CA/Rh(0)	156	0.6	4.5	5.9
7	CA/1.0gIL/Rh(0)	91	0.3	5.7	4.3

[a] Using 10 mg of Rh(0) and Pt(0).

Table 4. Hydrogenation of Cyclohexene with CA/IL/Rh(0) and CA/IL/Pt(0) Using Different Concentrations of BMI·$N(Tf)_2$[a]

entry	sample	thickness (μm)	time (h)[b]	metal(0) (mg)	BMI·$N(Tf)_2$ (g)	TOF[b] (h^{-1})
1	CA/IL/Rh(0)	10	1.6	0.084	1.0	961
2	CA/IL/Pt(0)	10	1.4	0.084	1.0	2083
3	CA/IL/Rh(0)	40	0.5	0.168	1.0	1562
4	CA/IL/Pt(0)	40	0.6	0.147	1.0	2777
5	CA/IL/Rh(0)	20	0.7	0.168	0.2	1095
6	CA/IL/Rh(0)	20	0.2	0.168	0.5	3906
7	CA/IL/Rh(0)	20	0.3	0.168	1.0	2551
8	CA/IL/Pt(0)	20	0.3	0.168	0.2	4807
9	CA/IL/Pt(0)	20	0.2	0.168	0.5	7353
10	CA/IL/Pt(0)	20	0.6	0.168	1.0	2451
11	IL/Rh(0)		0.032	5.0	1.0	833
12	IL/Pt(0)		0.15	5.0	1.0	329
13	CA/IL	40	4.0	0.0	1.0	0

[a] Reaction conditions: membrane CA/IL/metal(0): 210 mg; cyclohexene 12.5 mmol, 4 bar of H_2, 75 °C. [b] Time for 10% cyclohexene conversion (determined by GC).

cellulose macromolecules resulted in a higher flexibility, lower viscosity, and a better formability of the cellulose.

The catalytic properties of the CA/IL/Rh(0) and CA/IL/Pt(0) membranes were evaluated in hydrogenation reactions of cyclohexene at 4 bar of H_2 and 75 °C (Table 4). The catalytic activity was highly influenced by the thickness of the membranes. For example, higher catalytic activity (TOF) was observed with 20 μm membranes employing 1.0 g of the IL compared to the 10 μm membranes (compare entries 1, 3, and 7 for Rh(0) and entries 2, 4, and 10 for Pt(0) in Table 4, see also Figures S6 and S7). This is probably related to the relatively low stability of the 10 μm films, which undergo agglomeration during the hydrogenation, thus reducing the exposed area of the catalytically active species.

It is clear from the TOF data that the CA/IL/Pt(0) membranes are more active than those without the cellulose (compare entries 9 and 12 of Table 4, for example). This is another indication that there is a synergistic effect between the cellulose and the IL on the stabilization of the nanoparticles. This result is in line with those results observed for other supported IL phase catalysts.[3] It is also evident that the best relation between the two materials is 0.5 g of the IL and 5.0 g of cellulose acetate (compare entries 5, 6, and 7 and 8, 9, and 10 of Table 4 for Rh(0) and Pt(0) 20 μm thickness films, respectively). This is probably related to membrane pore saturation with higher molar concentrations of the IL. Therefore, levels of 0.5 g/5.0 g IL/cellulose acetate guarantee nanoparticle stabilization and, most likely, the establishment of a more efficient porous contact region between the gas and the liquid phases within the membrane structure.[24] Of note, the CA/IL/Pt(0) material can be reused up to 2 times in the cyclohexene hydrogenation without loosing its catalytic activity.

Conclusion

The use of dispersed Pt(0) or Rh(0) nanoparticles in IL in conjunction with cellulose acetate generated functionalized membrane films in which the mechanical, thermal, and chemical stability was related to the amount of IL used. The augmentation of the IL content resulted in an increase of elasticity, decrease in tenacity and toughness (area under the stress−strain curve), and reduction of Young's modulus. However, the stress at break was not influenced by the IL content in the case of the Pt(0) samples. Therefore, the introduction of the IL is probably causing an increase in the distance between the cellulose macromolecules that results in a higher flexibility, lower viscosity, and better formability of the cellulose material. The nanoparticle/IL/cellulose acetate combination exhibits an excellent synergistic effect that enhances the activity and durability of the catalyst for the hydrogenation of cyclohexene.

Acknowledgment. Thanks are due to the following Brazilian Agencies: CNPq, CAPES, and FAPERGS for fellowships and partial financial support.

Supporting Information Available. Detailed material characterization data (IR spectra, TEM micrographs, and XRD) and catalytic experiments. This material is available free of charge via the Internet at http://pubs.acs.org.

References and Notes

(1) Mehnert, C. P.; Mozeleski, E. J.; Cook, R. A. *Chem. Commun.* **2002**, 3010–3011.

(2) Mehnert, C. P. *Chem.—Eur. J.* **2004**, *11*, 50–56.
(3) Riisager, A.; Fehrmann, R.; Flicker, S.; van Hal, R.; Haumann, M.; Wasserscheid, P. *Angew. Chem., Int. Ed.* **2005**, *44*, 815–819.
(4) Riisager, A.; Fehrmann, R.; Haumann, M.; Wasserscheid, P. *Top. Catal.* **2006**, *40*, 91–102.
(5) Riisager, A.; Eriksen, K. M.; Wasserscheid, P.; Fehrmann, R. *Catal. Lett.* **2003**, *90*, 149–153.
(6) Riisager, A.; Fehrmann, R.; Wasserscheid, P.; van Hal, R. *Ionic Liquids IIIB: Fundamentals, Progress, Challenges And Opportunities: Transformations And Processes*; Oxford University Press: New York, 2005; *902*, pp 334−349.
(7) Riisager, A.; Wasserscheid, P.; van Hal, R.; Fehrmann, R. *J. Catal.* **2003**, *219*, 452–455.
(8) Bianchini, C.; Giambastiani, G. *Chemtracts* **2003**, *16*, 301–309.
(9) Riisager, A.; Fehrmann, R.; Haumann, M.; Wasserscheid, P. *Eur. J. Inorg. Chem.* **2006**, *69*, 5–706.
(10) Feng, C. L.; Wang, Y. H.; Jin, Z. L. *Prog. Chem.* **2005**, *17*, 209–216.
(11) Mehnert, C. P.; Cook, R. A.; Dispenziere, N. C.; Afeworki, M. *J. Am. Chem. Soc.* **2002**, *124*, 12932–12933.
(12) Webb, P. B.; Kunene, T. E.; Cole-Hamilton, D. J. *Green Chem.* **2005**, *7*, 373–379.
(13) Gelesky, M. A.; Chiaro, S. S. X.; Pavan, F. A.; dos Santos, J. H. Z.; Dupont, J. *Dalton Trans.* **2007**, 5549–5553.
(14) Coronas, J.; Santamaria, J. *Catal. Today* **1999**, *51*, 377–389.
(15) Bottino, A.; Capannelli, G.; Comite, A.; Del Borghi, A.; Di Felice, R. *Sep. Purif. Technol.* **2004**, *34*, 239–245.
(16) Centi, G.; Perathoner, S. *Catal. Today* **2003**, *79*, 3–13.
(17) Zaman, J.; Chakma, A. *J. Membr. Sci.* **1994**, *92*, 1–28.
(18) Fritsch, D.; Bengtson, G. *Catal. Today* **2006**, *118*, 121–127.
(19) Ozdemir, S. S.; Buonomenna, M. G.; Drioli, E. *Appl. Catal., A* **2006**, *307*, 167–183.
(20) Kragl, U.; Dwars, T. *Trends Biotechnol.* **2001**, *19*, 442–449.
(21) Belyakova, L. A.; Linkov, V. M.; Belyakov, V. N.; Bulavina, T. V. *Sep. Purif. Technol.* **1998**, *14*, 117–125.
(22) Tonkovich, A. L. Y.; Zilka, J. L.; Jimenez, D. M.; Roberts, G. L.; Cox, J. L. *Chem. Eng. Sci.* **1996**, *51*, 789–806.
(23) Cuffe, L.; MacElroy, J. M. D.; Tacke, M.; Kozachok, M.; Mooney, D. A. *J. Membr. Sci.* **2006**, *272*, 6–10.
(24) Xu, J.; Dozier, A.; Bhattacharyya, D. *J. Nanopart. Res.* **2005**, *7*, 449–467.
(25) Cai, J.; Kimura, S.; Wada, M.; Kuga, S. *Biomacromolecules* **2009**, *10*, 87–94.
(26) Bagheri, M.; Rodriguez, H.; Swatloski, R. P.; Spear, S. K.; Daly, D. T.; Rogers, R. D. *Biomacromolecules* **2008**, *9*, 381–387.
(27) El Seoud, O. A.; Koschella, A.; Fidale, L. C.; Dorn, S.; Heinze, T. *Biomacromolecules* **2007**, *8*, 2629–2647.
(28) Viswanathan, G.; Murugesan, S.; Pushparaj, V.; Nalamasu, O.; Ajayan, P. M.; Linhardt, R. J. *Biomacromolecules* **2006**, *7*, 415–418.
(29) Chiba, R.; Nishio, Y.; Sato, Y.; Ohtaki, M.; Miyashita, Y. *Biomacromolecules* **2006**, *7*, 3076–3082.
(30) Turner, M. B.; Spear, S. K.; Holbrey, J. D.; Daly, D. T.; Rogers, R. D. *Biomacromolecules* **2005**, *6*, 2497–2502.
(31) Migowski, P.; Dupont, J. *Chem.—Eur. J.* **2007**, *13*, 32–39.
(32) Gelesky, M. A.; Umpierre, A. P.; Machado, G.; Correia, R. R. B.; Magno, W. C.; Morais, J.; Ebeling, G.; Dupont, J. *J. Am. Chem. Soc.* **2005**, *127*, 4588–4589.
(33) Scheeren, C. W.; Machado, G.; Teixeira, S. R.; Morais, J.; Domingos, J. B.; Dupont, J. *J. Phys. Chem. B* **2006**, *110*, 13011–13020.
(34) Cassol, C. C.; Ebeling, G.; Ferrera, B.; Dupont, J. *Adv. Synth. Catal.* **2006**, *348*, 243–248.
(35) Campos, E. A.; Gushikem, Y. *J. Colloid Interface Sci.* **1997**, *193*, 121–126.
(36) Kwon, J. W.; Yoon, S. H.; Lee, S. S.; Seo, K. W.; Shim, I. W. *Bull. Korean Chem. Soc.* **2005**, *26*, 837–840.
(37) Rodrigues, U. P.; Gushikem, Y.; Goncalves, M. D.; Cachichi, R. C.; deCastro, S. C. *Chem. Mater.* **1996**, *8*, 1375–1379.
(38) Feldman, J.; Orchin, M. *J. Mol. Catal.* **1990**, *63*, 213–221.
(39) Barrett, E. P.; Joyner, L. G.; Halenda, P. P. *J. Am. Chem. Soc.* **1951**, *73*, 373–380.
(40) Brunauer, S. *Langmuir* **1987**, *3*, 3–4.
(41) Zhu, S. D.; Wu, Y. X.; Chen, Q. M.; Yu, Z. N.; Wang, C. W.; Jin, S. W.; Ding, Y. G.; Wu, G. *Green Chem.* **2006**, *8*, 325–327.

BM9003089